CrossMark

ORIGINAL PAPER

HVOF and Laser-Cladded Fe–Cr–B Coating in Simulated Biomass Combustion: Microstructure and Fireside Corrosion

Liam Reddy[1] · Philip Shipway[1] · Colin Davis[2] · Tanvir Hussain[1] (iD)

Abstract Biomass is often considered as a low carbon alternative to fossil fuels in the power industry. However, the heat exchangers in biomass plants can suffer from chloride-based aggressive fireside corrosion. A commercially available amorphous Fe–Cr–B alloy was deposited onto a stainless steel substrate by HVOF thermal spray and laser cladding. The controlled environment corrosion tests were conducted in a HCl-rich environment at 700 °C for 250 h with and without KCl deposits. The samples were examined with XRD, SEM and EDX mapping to understand the corrosion mechanisms. In the absence of any deposits, the amorphous HVOF coating performed very well with a thin oxide growth, whereas the crystalline laser cladding suffered from ~ 350 μm metal loss. The scales were composed of $MnWO_4$, Fe_2O_3, Fe_3O_4 and Cr_2O_3. When a KCl deposit was present, the HVOF-sprayed coating delaminated from the substrate and $MnCl_2$ was found in the scale.

Keywords Biomass · Laser cladding · HVOF · Fe–Cr–B

✉ Tanvir Hussain
   tanvir.hussain@nottingham.ac.uk

   Liam Reddy
   liam.reddy@nottingham.ac.uk

   Philip Shipway
   philip.shipway@nottingham.ac.uk

   Colin Davis
   colin.davis@uniper.energy

1 Faculty of Engineering, The University of Nottingham, University Park, Nottingham NG7 2RD, UK

2 Materials and Corrosion Team, Technology Centre, Uniper Technologies Limited, Ratcliffe on Soar, Nottingham NG11 0EE, UK

🙲 Springer

Introduction

As a greenhouse gas, CO_2 is a major contributor to global warming. National and international legislation is in place with the aim of reducing the amount of CO_2 emitted [1]. The power industry, as a major producer of CO_2, is under pressure to decrease emissions whilst also increasing the efficiency of generation. One approach taken is to replace fossil fuels with biomass as a feedstock in conventional steam-generating units. Biomass is often considered a carbon neutral fuel source as the CO_2 it releases is offset by the CO_2 captured during its lifetime [2].

Fireside corrosion is the major cause of boiler down time in all industrial boilers, but particularly in those firing biomass [3]. A loss of material from the heat exchange surfaces can lead to component failure, either as a direct result of this metal loss, or through mechanical failure instigated by the formation of cracks [4]. The combustion of biomass can lead to the formation of corrosive combustion gasses such as chlorides as well as aggressive deposits on the heat exchange surfaces. This is a major cause of fireside corrosion in biomass-fired power plants [5]. An approach currently taken to reduce fireside corrosion resulting from the combustion of biomass is to operate boilers at a lower temperature where the degree of fireside corrosion is acceptable [6]. Another approach is to use corrosion resistant nickel-based alloys or other protective coatings and claddings to minimize wastage without the drop in efficiency associated with a lower operating temperature. There are a range of surface engineering techniques that can be used to produce these coatings, each with their own benefits.

High-Velocity Oxy-Fuel (HVOF) spray is a thermal spray process in which a combustible fuel is fed into the combustion chamber of the spray gun along with oxygen. In the chamber, the fuel is burnt and the hot expanding gas is forced out of the nozzle at supersonic velocities. The powder feed stock is fed into the spray plume, where the particles are melted and accelerated. HVOF thermal spray-deposited coatings have a lamellar microstructure built up as molten particles deform on impact with the substrate [7]. Porosity caused when splats do not completely match the geometry of the layer below is a problem as it provides a path for corrosion [8]. One of the major advantages of thermal spray processes over other coating techniques is that the particles solidify very rapidly without causing excessive heating to the substrate. The small powder particles are able to very rapidly disperse their heat into the substrate, resulting in rapid solidification rates on the order of 10^6 K s^{-1} [8]. These rapid solidification rates mean that, when compared to other coating techniques, it is possible to retain a much higher amorphous fraction, something which is suggested to improve corrosion resistance [9]. The rapid solidification rate also acts to limit grain growth, with grain sizes typically not exceeding 5 μm [7].

Another alternative coating technique is laser cladding. Laser cladding is a weld-type coating technique which involves using a high powered laser aimed on the surface of the substrate to create a meltpool. The feedstock material is fed, or placed into the laser spot and once in the laser beam, melts and combines with the substrate. On moving out of the laser spot, the newly formed clad bead is allowed to

cool, solidifying to produce the clad [10]. Laser cladding will typically produce a dense, well-adhered coating with low porosity. The laser-cladding process described above lays down a single track. To create a coating, multiple tracks must be laid side by side to produce a continuous layer. If the track geometry is too circular, or there is not enough overlap, voids can occur at the interpass boundary [11].

Current material choices for heat-exchanger coatings are Ni–Cr-based alloys, such as Inconel 625. There is obvious economic incentive to using Fe-based alloys as they offer a cheaper alternative to conventionally used Ni-based alloys. In this study, Fe–Cr–B alloy was deposited by both HVOF thermal spray and laser cladding onto a 304 stainless steel substrate. This is a metallic glass forming alloy and by coating with two different methods: thermal spray and laser cladding, known to produce markedly different microstructures, the effects of these microstructures on the high-temperature corrosion were investigated. The novelty of this study lies in the direct comparison of the high-temperature corrosion performance of the two coatings with different amorphous phase fractions.

After deposition, the coatings were then exposed to a high-temperature, controlled environment fireside corrosion test to simulate biomass combustion conditions, in the presence of KCl deposits for 250 h at 700 °C. The morphologies and composition of the corroded samples were examined in an SEM with EDX with additional compositional information gained from XRD analysis. Finally, the performance of the coatings was examined on the polished cross section.

Experimental Procedures

A commercially available feedstock powder Weartech$^\circledR$ SHS^{TM} 7574 (The Lincoln Electric Company, OH), with composition (B = 2.96, Cr = 17.78, Mn = 2.10, Mo = 14.24, W = 5.90, C = 0.88, Al < 0.05, Co = 0.06, Cu = 0.09, Nb < 0.02, Ni = 0.13, P = 0.016, Si = 1.36, Sn < 0.02, Ta < 0.02, Ti < 0.02, V = 0.05 and Fe balance all in wt%), measured by AMG Analytical Services, was deposited by HVOF thermal spray and laser cladding onto a 304 stainless steel substrate (C < 0.08, Cr < 20, Mn < 2, Ni < 12, N < 0.1, P < 0.045, Si < 0.75, S < 0.03 and Fe balance all in wt%). The powder had a size fraction of +15 to 53 μm with an average particle size of 40.0 μm, and 10% of particles were smaller than 23.8 μm and 90% smaller than 66.6 μm. This was measured using a Mastersizer 3000 (Malvern Instruments, UK). A Met-Jet 4L (Metallisation Ltd, UK) HVOF thermal spray was used to deposit the powder onto 60 mm × 25 mm × 3 mm coupons of substrate. This is a kerosene-fuelled gun where the powders are injected downstream of the nozzle at a rate of 0.45 L min^{-1}, with an O_2 flow rate of 862 L min^{-1}. Before deposition, the coupons were grit blasted with F100 mesh brown alumina grit and degreased with industrial methylated spirit. The samples were mounted on a rotary carousel with a vertical axis of rotation, and the spray gun traversed the sample surface along the vertical direction at a scan rate of 5 m s^{-1}. The speeds were selected as to provide an interpass distance of 4 mm.

A 2-KW Ytterbium-doped fibre laser (IPG Photonics, Germany) with a 600-μm fibre was used to deposit the same feedstock onto a 200 mm × 100 mm × 6 mm 304 stainless steel plate. This gave a spot size of 4 mm when used with a 20 mm defocus. A power of 800 W and a traverse speed of 300 mm min^{-1} were used to deposit the clad.

A high-temperature, controlled environment corrosion test was performed in a horizontal tube furnace with an internal diameter of 70 mm. The stainless steel reactor used in the furnace was lined with alumina, and the samples were placed in individual alumina crucibles. The dimensions of the samples for the fireside corrosion tests were 10 mm × 10 mm. The test environment contained 500 ppm HCl, 5% O_2 and N_2 balance at a flow rate at room temperature of 35 cm^3 min^{-1} for 250 h at 700 °C. Although this temperature is higher than the conditions that would be experienced in a typical biomass boiler, they were selected so that an appreciable loss could be measured over a short test period.

Before exposure, the samples were degreased and cleaned using ultrasonic agitation in industrial methylated spirit. The samples were split into two groups, each containing a HVOF-sprayed sample and a laser-clad sample. A mixture of 10% KCl in industrial methylated spirit slurry was applied on the sample surface with a brush, which after drying deposited an average of 14 ± 1 mg of KCl on each sample. The second group of samples was prepared with no deposit. The samples were placed in ceramic crucibles and weighed before exposure. After exposure, the samples were weighed again so the mass gain could be calculated.

X-ray diffraction was used to examine the phases present in the top surface of the samples, both before and after exposure, on a D500 Diffractometer (Siemens AG, Germany) with a diffracted-beam monochromator and scintillation counter detector. The instrument was operated at 40 kV and 20 mA to generate Cu Kα radiation at a wavelength of 0.1540 nm. The XRD scans were performed in the range $30° \leq 2\theta \leq 90°$ with a step size of 0.08° and a step dwell time of 8 s. Typical samples for the XRD studies had a surface area of 10 mm × 10 mm.

For the microstructural analysis, the as-sprayed and exposed samples were mounted in cold-mounting resin filled with ballotini for low shrinkage, and the cross-sectional ground and diamond polished to a 1-μm finish. Backscattered Electron images were taken of both the top surface and cross section of each sample on an S-3400N SEM (Hitachi High Technologies, IL) in variable pressure mode with a 20 kV beam voltage. This was accompanied by Energy-Dispersive X-ray Spectrometry on an x-max 80 mm^2 spectrometer (Oxford Instruments, UK) to determine the composition of the scales.

Results and Discussion

As-Deposited Coatings

Figure 1 shows the phases that were present in the feedstock powder, the as-sprayed, and the as-clad material. The powder was predominantly amorphous with a broad hump, a typical feature of metallic glasses, seen centred around 44° [12].
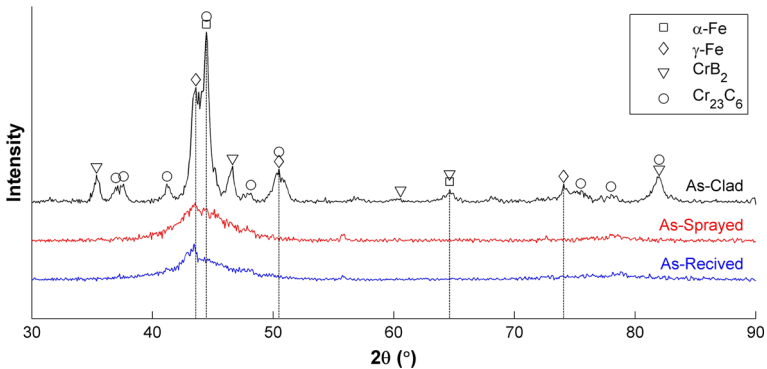
Fig. 1 XRD of Weartech® SHS™ 7574 powder as-received, after coating with HVOF onto a 304 stainless steel substrate and after laser cladding onto a 304 stainless steel substrate

Whilst there were no clearly defined peaks, the broad amorphous hump is centred on a γ-Fe reflection suggesting that some fraction of the powder had a crystalline structure.

The XRD of the HVOF-sprayed coating showed a slightly broader hump, with a less well-defined peak, corroborating the proposed beneficial effects of HVOF spray in retaining amorphous fraction in metallic glass feedstocks. The literature suggests that thermal spray can retain the amorphous fraction in the feedstock [7, 13–15]. It is suggested that this effect is due to the rapid cooling rates that occur when the molten particles from the spray process are incident on the substrate, on the order of 10^6 k s^{-1} [8]. Although after HVOF spray the coating became more amorphous, the characteristic peak of α-Fe became visible. This appearance of ferrite is consistent with the process of melting and resolidification of the austenite phase observed in the as-received powder.

The laser-cladding process removed some of the amorphous fraction observed in the as-received powder. The two most prominent peaks in the XRD were still those of the γ-Fe and α-Fe phases. There was also obvious formation of CrB_2 and $Cr_{23}C_6$. Whilst the peaks were more defined, the patterns were much more diffuse than would be expected from a fully crystalline structure, suggesting some amorphous fraction had been retained.

Cross-Sectional Examination and Mass Change

As-deposited coating cross sections can be seen in Fig. 2. The mean coating thickness before exposure was measured to be 235 ± 4 μm for the HVOF-sprayed coating and 732 ± 20 μm for the laser cladding. The HVOF coating was well bonded to the substrate, and there were no interfacial cracks present at the interface. Occasional porosities were noticed at the splat boundaries as well as within the splat. The laser cladding was metallurgically bonded to the substrate, and there were some gas pores present. Some mixing of the substrate is observed between tracks. Figure 3 shows the cross section of the coatings after exposure both without any
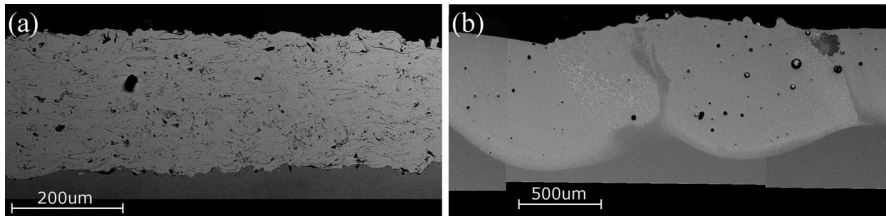
Fig. 2 BSE images showing the cross-sectional microstructure of the **a** HVOF-sprayed coating and **b** laser cladding
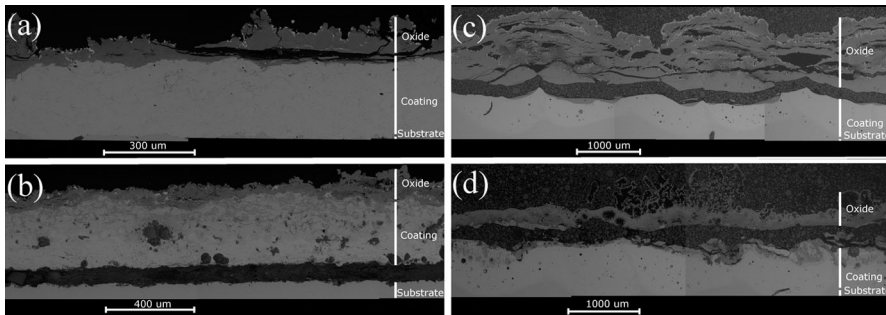
Fig. 3 BSE images showing the cross-sectional microstructure of the **a** HVOF-sprayed coating with no deposit, **b** HVOF-sprayed coating with KCl deposit, **c** laser cladding with no deposit and **d** laser cladding with KCl deposit

deposit and with the KCl deposit at 700 °C for 250 h. The average thickness of the HVOF-sprayed coating without any deposit was 274 ± 3 μm, and with KCl deposit was 276 ± 7 μm. This minimal change in thickness has been observed in similar Fe–Cr–B coatings under similar conditions [16]. The laser cladding was strongly affected by the exposure, with an average coating thickness of 381 ± 24 μm for no deposit and 557 ± 33 μm for the KCl deposit. The HVOF-sprayed coating after exposure with KCl delaminated from the substrate.

Traditional mass gain data were also recorded for comparison with the literature. The mass gain per unit area of the laser-clad samples was greater than that of the HVOF-sprayed samples both with the KCl and with no deposit. This shows that HVOF-sprayed samples had a lower oxide formation rate than laser-clad samples in these two environments. The HVOF-sprayed samples showed a mass change per unit area of 43.12 mg cm^{-2} with no deposit and 130.89 mg cm^{-2} with the KCl deposit with an average scale thickness of 80 ± 17 and 66 ± 8 μm, respectively. These were lower than the observed mass change per unit area of the laser-clad samples which were 153.38 mg cm^{-2} with no deposit and 166.91 mg cm^{-2} with the KCl deposit. The thicknesses of these oxides were 986 ± 63 μm with no deposit and 328 ± 49 μm with a KCl deposit. This observation was consistent with the proposed benefits of an amorphous microstructure in improving corrosion performance as outlined above.

## Characterization of Corrosion Products

XRD analysis of the exposed coatings is shown in Fig. 4. The integrity of the HVOF-sprayed coating with KCl deposit was poor, and it was not possible to use XRD on that sample. Both the HVOF-sprayed and laser-clad samples showed strong reflections from $MnWO_4$, when no deposit was present. This oxide was not detected on the surface of the laser cladding with a KCl deposit. $MnWO_4$ reacts with gaseous Cl_2 to form $MnCl_2$ and WO_2Cl_2 [17]. No chlorides were detected on the surface of the samples without any deposit, suggesting that HCl from the gas did not react to form chlorides, and instead the KCl deposit was providing the gaseous Cl_2 needed for the removal of $MnWO_4$. Cr_2O_3 is another phase that was observed in both the HVOF-sprayed and laser-clad samples without any deposit, but not when KCl was present. The phase most dominant across all of the samples, however, was Fe_2O_3. On the laser-clad sample with the KCl deposit, the only other major phase identified other than Fe_2O_3 was Fe_3O_4. It is well established that Fe_2O_3 and Fe_3O_4 are much less protective than Cr_2O_3. This suggests when KCl was involved the clad material, with 25 wt% Cr, failed to form a protective chromia layer.

Figure 5 shows the cross-sectional images of both the samples without any deposit and corresponding EDX maps. Figure 5a shows a thick dark contrast oxide layer with a bright oxide phase on top. The external oxide layer was mainly composed of Fe and O with a small amount of Cr. This is likely to be a combination of Fe_2O_3 and Fe_3O_4 as determined by XRD. The Cr_2O_3, which was also detected in XRD, is underneath the Fe-rich oxide. $MnWO_4$ was located on the top surface of the Fe-rich oxide. Cl was not detected in EDX maps in the cross section, suggesting that HCl did not react with the coating to form any chlorides.

The laser-clad sample is shown in Fig. 5b. The scale thickness was significantly more than that of the HVOF-sprayed sample. It showed many of the same phases as those found in the HVOF-sprayed sample. The oxide layer was mainly composed of Fe, Cr and O, with the Cr present in higher quantities towards the scale-coating
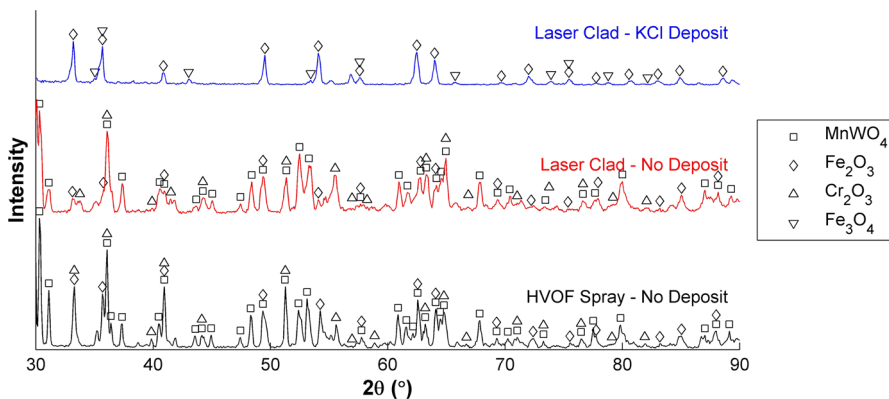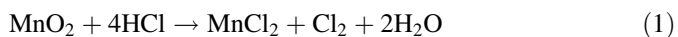

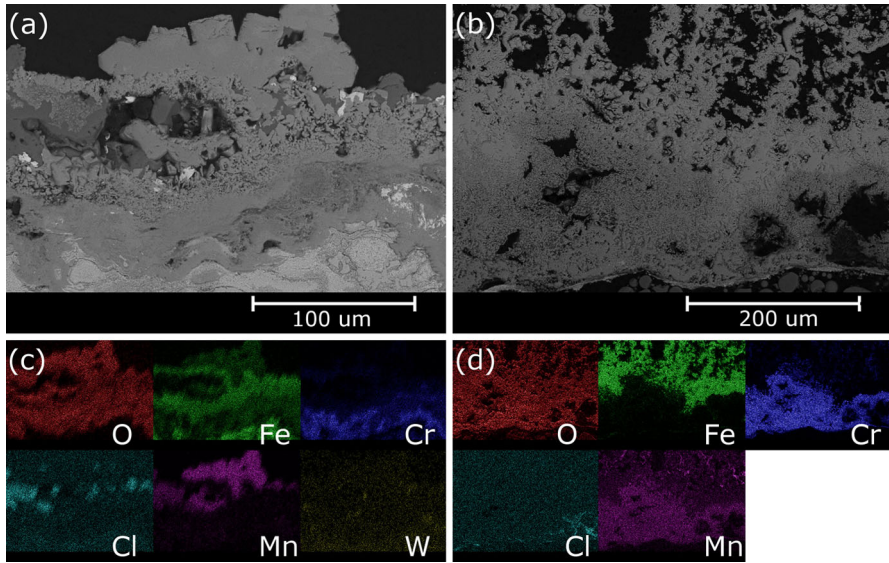**Fig. 4** XRD of HVOF and laser-clad samples after exposure
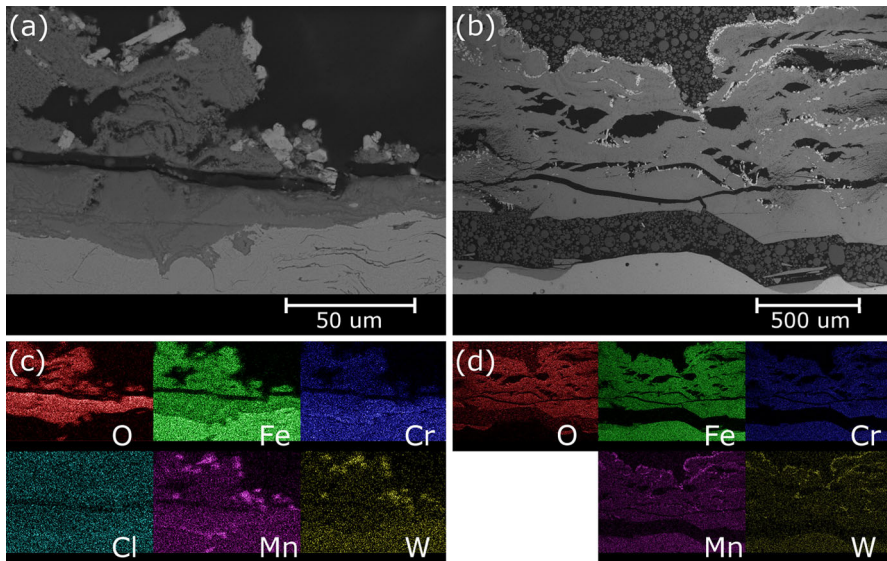
Fig. 5 Cross-sectional BSE images of the HVOF-sprayed (**a**) and laser-clad (**b**) samples after 250 h at 700 °C with no deposit. The corresponding EDX maps are shown in **c** for HVOF coating and **d** for laser cladding

interface. EDX analysis of these regions showed the oxides were likely of the same composition as those found in the HVOF-sprayed sample. $MnWO_4$ was also present in the scale of the laser-clad sample, as was confirmed with EDX mapping and XRD.

The cross-sectional images of the samples with deposits are shown in Fig. 6. When comparing these cross sections to those with the KCl deposit, the most noticeable difference was the presence of Cl in the scales. Mn and O were detected on the outside of the scale with a Fe-rich oxide formed underneath. EDX maps showed another Mn-rich layer contained Cl embedded within this Fe-rich oxide. EDX spot analysis suggested its composition is close to $MnCl_2$. One mechanism for the formation of $MnCl_2$ is through MnO_2 interacting with HCl via Eq. (1) [18]. This formation process is corroborated by the presence of Mn and O which is seen in Fig. 6a as the cubic, fan-like structure at the surface of the sample.

$$MnO_2 + 4HCl \rightarrow MnCl_2 + Cl_2 + 2H_2O \qquad (1)$$

Unlike the samples with no deposits seen in Fig. 5, these KCl-covered samples did not show the $MnWO_4$ phase. A Cr-rich oxide formed underneath the $MnCl_2$. This Cr-rich layer did not contain any Fe, although no Cr_2O_3 was detected in the XRD due to the thickness of the mixed corrosion products. The laser-clad sample after 250-h exposure is shown in Fig. 6b where the mixed corrosion product layer was observed to be over 300 µm thick. The outer oxide was a Fe-rich oxide which was porous at the top. The Cr was only detected below the Fe oxide, an area which

Fig. 6 Cross-sectional BSE images of the HVOF-sprayed (**a**) and laser-clad (**b**) samples after 250 h at 700 °C with KCl deposit. The corresponding EDX maps are shown in **c** for HVOF coating and **d** for laser cladding

also contains Mn. This was a mixture of Cr and Mn oxides although there was no Cr or Mn phase detected in the XRD due to the small penetration depth. Cl was detected underneath the oxide scales, suggesting that the scales were not protective in nature. Cl ions can migrate through the non-protective oxide readily.

Figure 7a, c showed the morphology of the oxide scales grown on the HVOF-sprayed coating and laser cladding without any deposit. In both cases, the bright phase in the BSE image was detected to be $MnWO_4$. The oxides were rod shaped and grew up to 20 μm in length on the HVOF-sprayed coating.

The top surface of the HVOF-sprayed coating with KCl deposit, Fig. 7b, showed two morphologically different phases. There was an iron oxide phase making up the bulk of the surface similar to all of the other samples; however, this sample was unique in that it had a second, diamond-shaped, iron oxide.

Similarly, there were two distinct textures that could be seen on the surface of the laser-clad sample with a KCl deposit, Fig. 7d. Small globular-shaped oxides formed the majority of the sample surface, which comprised of Fe and O. EDX and XRD analysis showed it to be Fe_2O_3. EDX analysis did not detect any Cr, suggesting this was a very thick region of Fe_2O_3. The other region seen on the bottom of Fig. 7d showed this is a mix of Fe_2O_3 and Cr_2O_3.
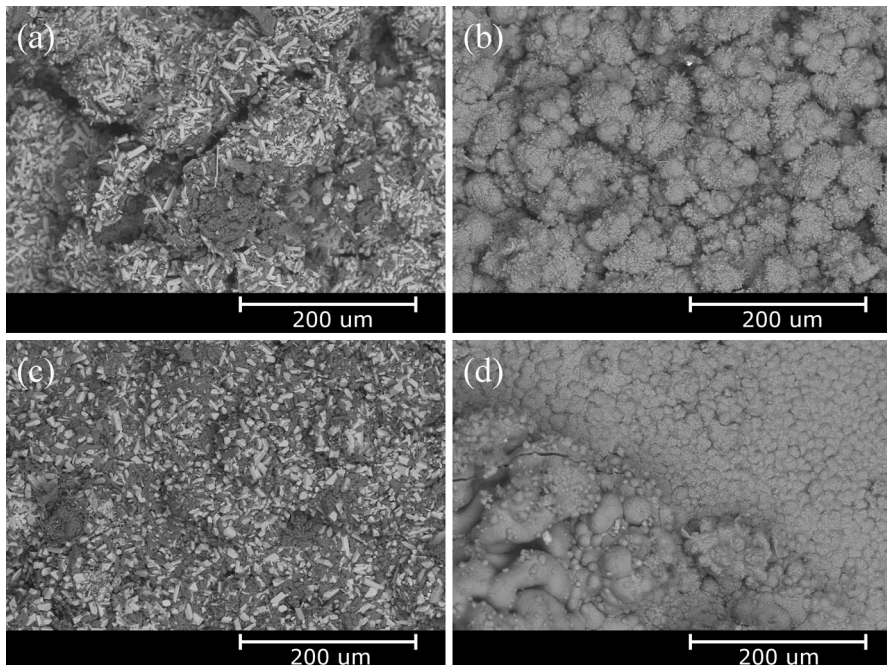
Fig. 7 Top surface after 250 h in 500 ppm HCl, 5% O_2, N_2 Bal. at 700 °C **a** HVOF spray with no deposit, **b** HVOF spray with KCl deposit, **c** laser cladding with no deposit, **d** laser cladding with HCl deposit

Conclusions

In this study, an amorphous Fe–Cr–B feedstock was deposited onto a heat-exchanger material using HVOF thermal spray and laser cladding. The aim was to understand the corrosion mechanisms of these coatings in a simulated biomass combustion environment. The coated samples were exposed in 500 ppm HCl + 5% O_2 at 700 °C for 250 h without any deposits and with KCl deposits. The following conclusions can be made:

HVOF thermal spray produced a predominantly amorphous microstructure retaining the phases in the feedstock powder. Laser cladding produced a predominantly crystalline structure with α-Fe, γ-Fe, CrB_2 and $Cr_{23}C_6$.

Both samples without deposits developed an oxide scale of $MnWO_4$, Fe_3O_4, Fe_2O_3 and Cr_2O_3. The thickness loss of the HVOF coating was negligible, but the laser-clad sample lost ~350 μm in 250 h. The mass gain of the laser-clad sample was three times higher than the HVOF-sprayed coating. The constituent microstructure played a key role in the corrosion behaviour in these environments. It can be concluded that a high amorphous fraction in the material can improve corrosion resistance.

MnCl$_2$ was detected in both samples when KCl deposit was used. The scales contained Fe$_3$O$_4$, Fe$_2$O$_3$; however, MnWO$_4$ was not formed. Cl was detected underneath the oxide scales due to a lack of protective scale formation.

Weartech® SHS^{TM} 7574 coating is a promising candidate coating for heat-exchanger components as protective Cr$_2$O$_3$ was formed under some conditions. Whilst the HVOF-thermal-sprayed coating showed better corrosion performance, the spallation of the coating could be a concern for use in real boiler conditions. Laser-cladded SHS 7574 coating is currently being exposed in a utility-scale biomass-fired power plant in the UK as a part of the field trial.

References

1. J. Skea and P. Ekins, *UKERC Energy 2050 Project: Making the Transition to a Secure and Low-Carbon Energy System: Synthesis Report*, Report No. S3097 (UKERC, 2009).
2. K. Tokimatsu, R. Yasuoka, and M. Nishio, *Applied Energy* **185**(2), 1899 (2017).
3. N. J. Simms, J. Sumner, T. Hussain and J. E. Oakey, *Materials Science and Technology* **29**(7), 804 (2013).
4. T. Hussain, A. U. Syed and N. J. Simms, *Fuel* **113**, 787 (2013).
5. R. W. Bryers, *Progress in Energy and Combustion Science* **72**, 29 (1995).
6. M. Oksa, S. Tuurna, and T. Varis, *Journal of Thermal Spray Technology* **22**(5), 783 (2013).
7. J. R. Davis, *Handbook of Thermal Spray Technology* (ASM International, Ohio, 2004).
8. S. J. Bull, J. O. Carlsson, P. R. Charlker, G. Dearnaley, K. S. Fancey, F. C. J. Fellowes, A. S. James, R. Kingswell, A. Leyland, A. Matthews, W. D. Munz, D. S. Rickerby, S. L. Rhode, S. M. Rossnagel, K. T. Scott, and W. M. Steen, *Advanced Surface Coatings: A Handbook of Surface Engineering* (London, 1991).
9. W. H. Wang, C. Dong and C. H. Shek, *Materials Science and Engineering R: Reports* **44**, 45 (2004).
10. W. M. Steen, *Laser Material Processing* (Springer, London, 1991).
11. E. Toyserkani, A. Khajepour, and S. Corbin, *Laser Cladding* (CRC Press, Boca Raton, 2004).
12. R. Babilas, M. Kadziolka-Gawel and A. Burian, *Journal of Non-Crystalline Solids* **435**, 76 (2016).
13. K. Chokethawai, D. G. McCartney, and P. H. Shipway, *Journal of Alloys and Compounds* **480**(2), 351 (2009).
14. M. Oksa and J. Metsäjoki, *Journal of Thermal Spray Technology* **24**(3), 436 (2015).
15. V. K. Balla and A. Bandyopadhyay, *Surface and Coatings Technology* **205**(7), 2661 (2010).
16. S. Tuurna, T. Varis, K. Penttila, S. Holmström, K. Ruusuvuori, S. Holmstro and S. Yli-Olli, *Materials and Corrosion* **62**, (7), 2011 (642).
17. G. C. Fouga, R. M. Taddeo, M. V. Bosco and A. E. Bohe, *Thermochimica Acta* **536**, 30 (2012).
18. V. S. Kolosnitsyn, E. A. Minnikhanova, E. V. Karaseva, Y. K. Dmitriev and M. M. Muratov, *Applied Electrochemistry and Corrosion Protection of Metals* **76**(6), 891 (2005).